Nanomanufacturing and Metrology
https://doi.org/10.1007/s41871-019-00051-5

ORIGINAL ARTICLES

In Situ Measurement of Spindle Radial and Tilt Error Motions by Complementary Multi-probe Method

Fei Ding[1] · Xichun Luo[1] · Wenlong Chang[1] · Zhengjian Wang[1]

Received: 13 September 2019 / Revised: 29 October 2019 / Accepted: 31 October 2019

Abstract
This paper presents a complementary multi-probe method for measurement of radial and tilt error motions of a spindle. Neither indexing of artefact nor rotating of spindle housing is required and thus make it suitable for in situ evaluation of spindle performance effectively. In order to minimize the harmonic suppression problems commonly encountered in the multi-probe measurement approach, three sets of probe angle combinations were optimized and the harmonics of the three measurements were extracted and composed to reveal the true artefact errors in a complementary way. The exact probe angles were identified by the correlation function of the probe signals after the sensors are mounted onto the fixture and the requirement of high-precision fixtures was alleviated. The evaluation of measurement results showed that the erroneous harmonics were greatly reduced by 70%. Using this method, the radial error motions of the precision air bearing spindle were measured at seven axial positions and then the synchronized tilts error motions were calculated. This demonstrated an effective approach for measuring four degree-of-freedom error motions in one setup with a small number of displacement sensor probes.

Keywords Spindle error · Multi-probe method · Precision spindle · Harmonic suppression

1 Introduction

Rotary motions can be found in the majority of machine tools and the study of spindle error motions has always been a necessity for machine tool manufacturers [1, 2]. Usually, a precise cylinder datum is mounted on the spindle rotor and the circumferential shape of the datum is treated as a perfect circle. This cylinder datum part is also called artefact in spindle metrology literature [3]. In ultra-precision machine tools, the spindle runout errors are as small as tens of nanometers, while the circularity error of the artefact can easily be larger. Therefore, the key issue of spindle metrology is to separate the true rotor error motions from the measured sensor data, which includes the circularity error of the artefact. Reversal, multi-probe and multi-step methods are the three most commonly used separation techniques for spindle metrology [4, 5]. Reversal method typically involves the repositioning of both the artefact and probes, which will inevitably introduce extra measuring uncertainties. An improved reversal method has been proposed by Grejda [3], where the spindle is rotated instead of the probe. However, the artefact and spindle rotor still need to be repositioned. The authors tried to alleviate this problem by designing a dedicated fixture using a spherical pilot mated in a carbide socket to locate the artefact. The fixture is very complicated and costly to make. Lee et al. [6] applied the reversal method to measure the spindle error motion for a large-scale machine tool and obtained the full error map of the roll workpiece. Marsh et al. compared the reliability of three separation methods and it shows that the multi-probe method gives comparable results to the reversal method [3, 7].

The multi-probe and multi-step methods have the same problem of harmonic suppression, which derives from the algorithm used to separate the artefact profile [8]. Using more sensors can reduce these effects but will increase the number of error sources and the cost. Zhang et al. [9, 10] investigated four-point and multi-point error separation methods in roundness measurement by computer simulation and concluded that measuring with more than four probes does not improve the measurement results much. Variations of the multi-point method have since been proposed. Chen et al. [11] proposed a novel three-probe

✉ Xichun Luo
xichun.luo@strath.ac.uk

[1] Department of Design, Manufacture and Engineering Management, Centre for Precision Manufacturing, University of Strathclyde, Glasgow G1 1XQ, UK

Published online: 11 November 2019

method by solving systems of multivariable equation (SSME) and verified it by both theoretical analysis and experiments. Linxiang et al. [12] modified the multi-step method by deploying three groups of equally angled indexations (7, 8, and 9) and claimed the full harmonic separation ability through simulation, but it has not been experimentally proved. Cappa et al. [13, 14] achieved 0.455-nm repeatability using only one probe in the multi-probe method by rotating the spindle stator and this method circumvents the error source caused by the inconsistency of sensitivities between sensor probes. However, the spindle housing has to be rotated, which is not always feasible in industrial conditions. Shi et al. [15, 16] proposed a hybrid multi-probe method where the weighting function coefficient is optimized from several measurements to reveal the spindle error motions and also studied the propagation of the measurement uncertainty but his experimental setup cannot achieve precise results due to sensor limitations. Zhao et al. [17] developed a single-step rotation error separation technique (SEST) by rotating the artefact a small angle. This method can remove harmonics singularity in the range of 1–100 UPR with only one rotation and thus saves measuring time. Tong proposed a two-step method different from the traditional multi-step method by applying Prony spectrum method and singular value decomposition to separate the errors [18].

New types of sensors are also used to gather as much information as possible. Gao et al. [19–21] proposed an enhanced configuration with the two-displacement-one-angle (2D1A) mixed method. Liu et al. [22] tried to measure the spindle errors by a specially designed optical sensor setup. The new sensors can help the separation of circularity error of the artefact, but this also increases the number of error sources.

Apart from the studies on error separation algorithms, some other researchers focused on the measurement apparatus design. Vissiere et al. [23] introduces the concept of dissociated metrological structure (DMT) for cylindricity measurement at a nanometric level of accuracy. Ashok et al. [24] carried out fixed sensitive radial error measurement of a high-speed spindle and the error sources are separated by DFT-based frequency domain filtering method. He used laser sensors to measure the errors but with limited resolution. Chen et al. [25] identified the spindle error motions through the evaluating the surface form of the machined parts with wavelet transform. However, the machined surface is the result of many factors and the surface form cannot fully reflect the spindle error motions. Ma et al. [26] applied three-point error separation method in hydrostatic spindle error measurement, which features online finish turning. Shu et al. [27] studied the measuring uncertainties resulting from sensor alignment and non-linearity for Donaldson reversal and three-point techniques.

Some of the above researchers have achieved very good measurement repeatability. However, those measurements are conducted in a controlled lab on specially designed setups. In most cases, after the spindle is mounted on a machine tool, rotation of the spindle stator is impossible, and precision reversal is not applicable. This paper presents a complementary multi-probe method which shows effective reduction of harmonic errors without requirement of repositioning of the artefact or the spindle, making it suitable for in situ measurement in production environments. The positions of the sensors still need to be changed but the true positions are detected through sensor signals after mounting, reducing the requirement on the fixture precision. Measurement experiments were conducted to verify this approach.

2 Methodology

2.1 Complementary Spindle Error Separation

In the complementary multi-probe setup as shown in Fig. 1, a cylindrical artefact is fixed to the spindle rotor and is rotated during the measurement cycle. A fixed probe fixture is used to position the sensor probes. The error motions of the spindle together with the imperfections of the artefact are detected by three displacement sensors. The artefact profile signal is imposed on the spindle error motion signals with different phases at different probe angles. The one-off measurement cannot separate the artefact errors effectively due to the harmonic suppression problem [8]. Then the probes are relocated into a different angle combination and another measurement is done. One probe is kept unchanged in order to get a fixed angular reference. The measurement can be done multiple times.

In each measurement, the instantaneous rotating center of the spindle is denoted as (x, y) in the fixed Cartesian coordinate, with the X-axis direction in line with the first probe. When the spindle rotates, this rotating center location keeps changing, which is observed to be the radial motion errors.s_1 ,s_2 and s_3 are displacements measured from three directions against the artefact, with relative angles of α and β from the X direction. $a(\theta)$ is the profile of the artefact around the circumference. In practice, the shape change of the artefact caused by thermal variation and centrifugal force is negligible. Thus, the circumference profile of the artefact is assumed to be constant throughout the measurement cycle. The relationships between the probe measurements and the errors are

$$s_1(\theta) = a(\theta) + x(\theta) \tag{1}$$

$$s_2(\theta) = a(\theta - \alpha) + x(\theta)\cos\alpha + y(\theta)\sin\alpha \tag{2}$$

$$s_3(\theta) = a(\theta - \beta) + x(\theta)\cos\beta + y(\theta)\sin\beta \tag{3}$$

Define the weighted summation of the probe signals $m(\theta)$ as

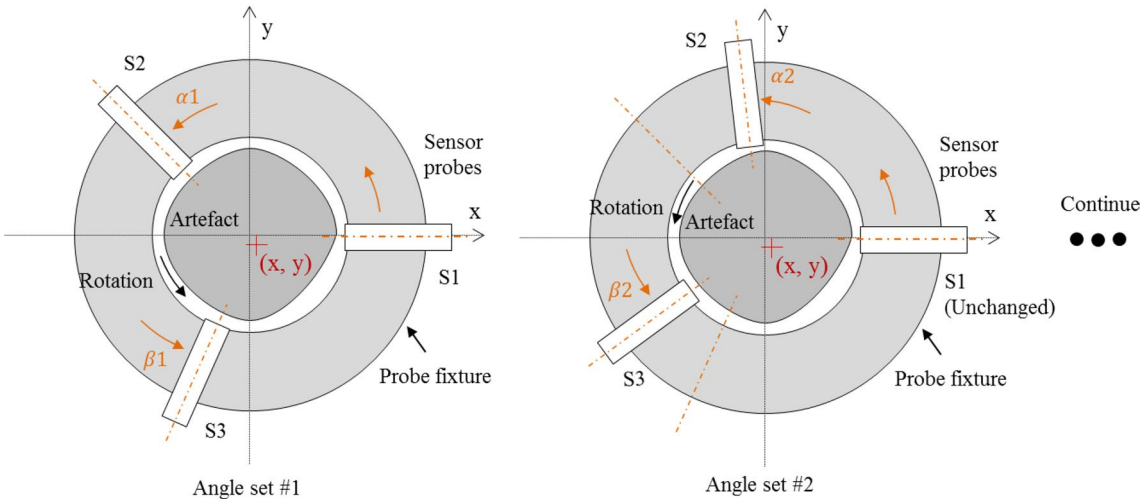

Fig. 1 Schematic diagram of the complementary multi-probe error separation method

$$m(\theta) = s_1(\theta) + c_1 s_2(\theta) + c_2 s_3(\theta) \tag{4}$$

The purpose is to make the value of $m(\theta)$ independent of the rotating center (x, y) by properly selecting the two weighting factors c_1 and c_2. Solving the equations of (1) to (3) and eliminating the $x(\theta)$ and $y(\theta)$, the following relationship holds:

$$\begin{aligned} s_1(\theta) - s_2(\theta)\frac{\sin(\beta)}{\sin(\beta-\alpha)} + s_3\frac{\sin(\alpha)}{\sin(\beta-\alpha)} &= a(\theta) \\ - a(\theta-\alpha)\frac{\sin(\beta)}{\sin(\beta-\alpha)} + a(\theta-\beta)\frac{\sin(\alpha)}{\sin(\beta-\alpha)} & \end{aligned} \tag{5}$$

By selecting the weighting factors as below

$$c_1 = \frac{-\sin\beta}{\sin(\beta-\alpha)} \tag{6}$$

$$c_2 = \frac{\sin\alpha}{\sin(\beta-\alpha)} \tag{7}$$

Then

$$m(\theta) = a(\theta) + c_1 a(\theta-\alpha) + c_2 a(\theta-\beta) \tag{8}$$

Apply Fourier transform on both sides and the transmit function from artefact error to summed probe signal can be derived as

$$G(k) = \frac{M(k)}{A(k)} = 1 + c_1 e^{-jk\alpha} + c_2 e^{-jk\beta} \tag{9}$$

This transfer function is called harmonic weighting function and k is the harmonic order. Then the artefact circularity error can be calculated in the harmonic domain by

$$A(k) = \frac{M(k)}{G(k)} \tag{10}$$

Since the weighting function appears in the denominator, a small value of $G(k)$ will amplify the measurement noises in $S(k)$. This is called the harmonic suppression problem in multi-probe method. The value of $G(k)$ at each harmonic depends on the angles of α and β. Thus, in this paper, several different groups of the angles α and β are applied in the measurements.

Assume that the harmonic weighting functions for different angle sets are $G_i(k)$ respectively, where i is the angle set number. The corresponding harmonics of the summed probe signals are $M_i(k)$ respectively. The summation and the weighting functions are used to calculate the artefact circularity error according to Eq. (10), resulting in n Fourier series of the artefact circularity error $A_i(k)$, where n is the total measurement number.

A complimentary processing approach is proposed in this paper to reconstruct the artefact circularity error from the multiple measurements. The different angles used in the measurements will result in harmonic suppressions at different harmonics. The erroneous harmonics in one error separation procedure can be corrected by the other measurements in which the same harmonics are not suppressed. The harmonic with the minimum amplitude at each harmonic bin is picked and then combined into a new Fourier series. The rationale behind this method is that the low values of G will only result in an amplification of the separated artefact error. Thus, the smallest harmonics are the least amplified ones.

$$A_{\text{comp}}(k) = \min\left(A_1(k), A_2(k), \ldots, A_n(k)\right),\ k = 1 \text{ to } \infty \tag{11}$$

Then the harmonics function $A_{\text{comp}}(k)$ is transformed into spatial artefact profile $a_{\text{comp}}(\theta)$ by inverse Fourier transform. Since each angle set result has its own corresponding phase values, the rearranged amplitudes can be used to obtain three results of the artefact form. The phase information is not

distorted by the low value of G and therefore all the measurements are meaningful. By solving Eqs. (1) and (2) with the obtained artefact error, the spindle radial errors in X and Y directions are calculated by

$$x(\theta) = s_1(\theta) - a_{\text{comp}}(\theta) \tag{12}$$

$$y(\theta) = [s_2(\theta) - a_{\text{comp}}(\theta - \alpha) - x(\theta)\cos(\alpha)]/\sin(\alpha) \tag{13}$$

2.2 Selection of Probe Angles

In this experiment, three sets of probe angle combinations are selected to optimize the minimum value of $|G|$. The angle set #1 is selected according to Cappa's research [14]. This angle set has been proven to be an optimal one for a single measurement. However, it still inevitably shows some small values. A MATLAB script is written to search for the other two angle values at which the three combinations do not compress the same harmonics. This is done by calculating the minimum G value at all the probe angles with angle step of 2°. The designed angle sets are listed in Table 1.

The absolute values of $G(k)$ at different harmonic orders for the three designed sets of angles are shown in Fig. 2. The minimum value is found of 0.1613 at 88 UPR for the second angle set.

Table 1 Designed probe angles for the complementary method

	Angle α(°)	Angle β(°)
Angle set #1	100.4000	230.0333
Angle set #2	141.0333	270.7050
Angle set #3	139.3667	239.1200

3 Experimental Design

The spindle under test is a precision air-bearing spindle mounted on a diamond turning machine as shown in Fig. 3. An aluminium cylinder artefact is first turned with a diamond tool on the machine, thus a small runout is guaranteed. A probe holder is designed with multiple square slots to position the capacitive probe as shown in Fig. 3. The probe mounting plate is adjusted perpendicular to the spindle rotating axis within 20 µm. The influences of probe positional error are analyzed in [28]. In order to reduce vibration, the air bearing slides are cut off from air supply and rested on the machine bed after positioning the probe holder. Three calibrated capacitive probes from Lion precision are used throughout the measurement. The bandwidth of the amplifier is adjusted to 1 kHz to achieve a resolution of 0.3 nm rms and the peak-to-peak resolution is expected to be ten times higher. A 16-bit eight-channel simultaneous sampling board is used to sample the displacement signal. The spindle is equipped with a 6000-line Heidenhain rotary encoder. The machine controller is configured to generate 10,000 pulses per revolution and these pulses are used to trigger the data acquisition device. Spindle speed is set to 60 rpm. Each test is started from the same spindle angular position from static and 200 consequent revolutions data are acquired. Because the spindle rotation is not stable during the start-up period, only the last 32 revolutions are used in the calculation.

Because the spindle also has tilt errors, which can be reflected by the radial error motions at different axial location, the measurement approach can be extended to measure the tilt error. The spindle error motion measurements are carried out at seven positions spaced by 21 mm along the axial direction (Z direction), each with three angular arrangements as shown in Fig. 4. The spindle

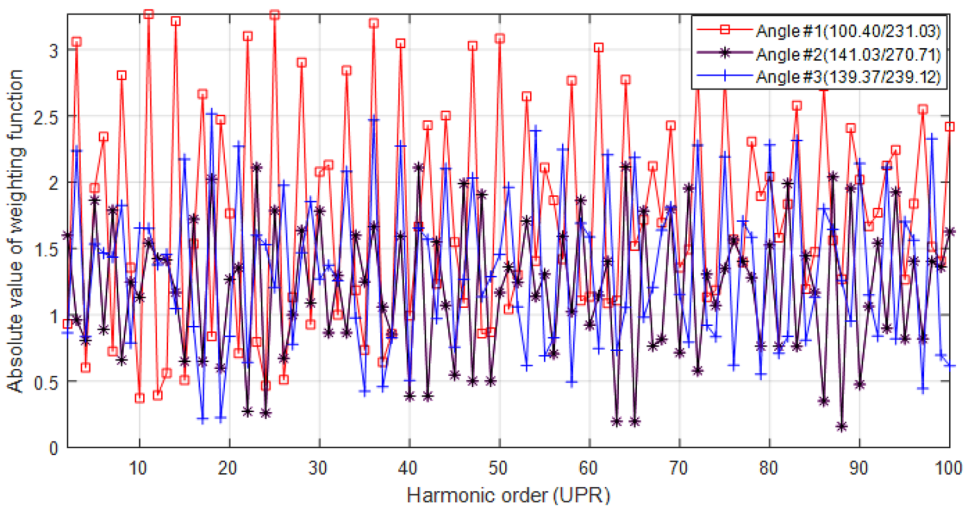

Fig. 2 Absolute values of $G(k)$ at different harmonic orders for the designed three sets of angles

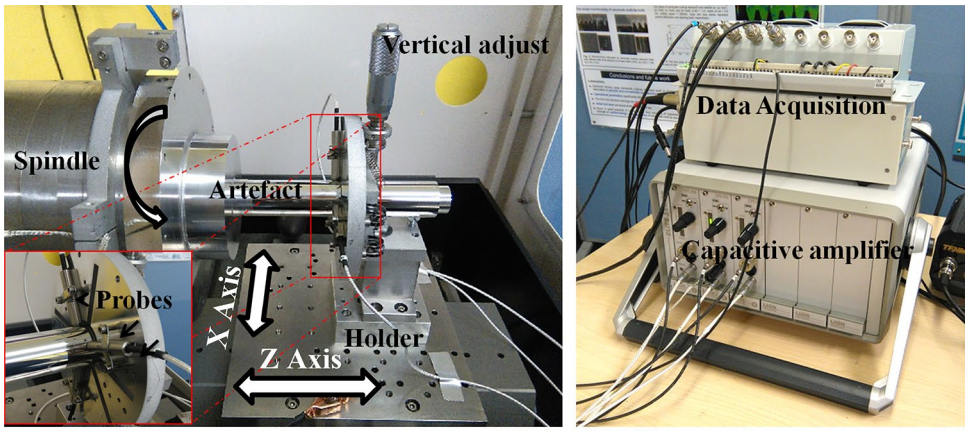

Fig. 3 Experimental setup for the spindle error measurement

(a) Measuring positions **(b)** Photo of experimental setup

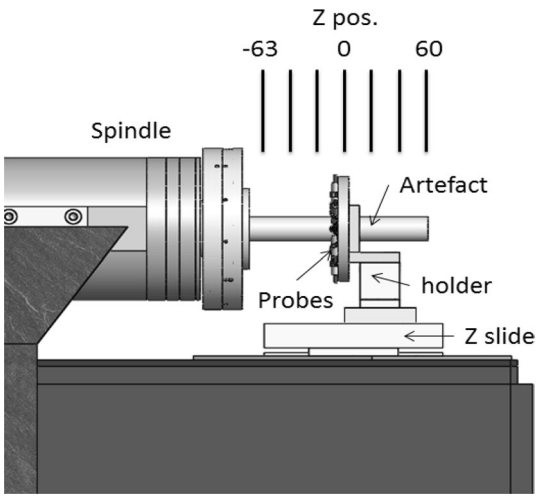

Fig. 4 Schematic diagram of the tilt error measurement method

error motions at different locations are later used to calculate spindle tilt errors by linear fitting.

4 Results and Discussion

The exact angles between the three probes are critical for the correct separation of artefact circularity error and spindle error motion. Although much effort has been put into selecting the different angles, there will be positioning errors when the probes are mounted on the sensor holder. The angle deviations will not be so large as to affect the overall shape of the weighting function, so the design process is still necessary. The question is how to determine the actual angles after the probes are mounted.

4.1 Determination of Probe Angles

In this experiment, a special mark on the artefact is used to determine the relative angle between probes. The outputs of the three probes pose the same profiles for the mark for every cycle with phase differences. Correlation function is used to find the relative phase angles. As the spindle error motion is superimposed onto the form profile including the designated mark, the mark feature has to be extracted before applying the correlation method. The extraction process is shown in Fig. 5. Firstly, the sensor output is filtered at 50-UPR cut-off frequency with zero-phase forward and reverse IIR filter. Then, an 8th-order polynomial is subtracted from the curve to remove the large wavelength while keeping the narrow mark signal dominates. After that, mark features for each probe are extracted with the same height from the peak, and mutual correlation is calculated to determine phase differences.

The angles are calculated once a cycle and 96 cycles are calculated in total. The actual probe angles are listed in Table 2, together with the standard deviations. The results show good repeatability with standard deviations within 0.03 degrees.

The three harmonic weighting functions calculated from the measured angles are shown in Fig. 6. Several unexpected small absolute values of G can be found at harmonics around 35 UPR and 60 UPR, which is not desirable. This also demonstrates the necessity for using more than one angle combination to recover components that are missed out in a single measurement.

4.2 Measurement of Spindle Radial Error Motions

Firstly, the measurement is conducted at one location, approximately 100 mm from the spindle bearing, with different angle sets to verify the frequency-domain modification approach. The interested harmonic range is set

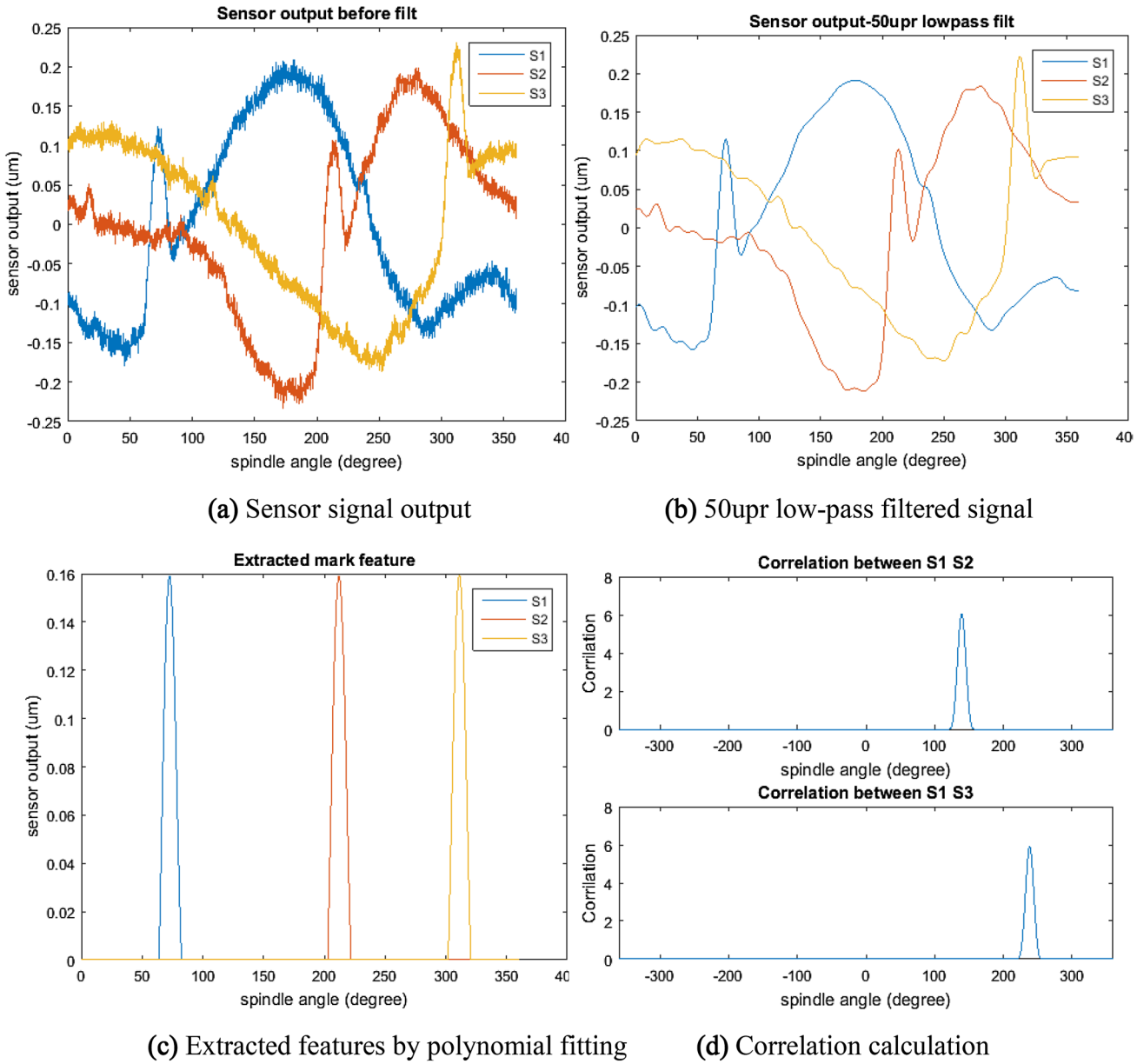

(a) Sensor signal output

(b) 50upr low-pass filtered signal

(c) Extracted features by polynomial fitting

(d) Correlation calculation

Fig. 5 Steps for calculation of actual probe angles with an ink mark

Table 2 Actual probe angles after probe mounting

	Angle α(°)	Standard deviation (°)	Angle β(°)	Standard deviation (°)
Angle set #1	100.15	0.0052	230.12	0.0314
Angle set #2	140.90	0.0052	269.92	0.0173
Angle set #3	139.33	0.0131	238.31	0.0144

as from 2 to 100 UPR and the asynchronous errors are removed by averaging 32 revolutions.

Figure 7a shows the separated artefact profiles with the traditional method from three measurements. The profile measured by angle set #1 shows much larger variations than angle set #2 and #3, which is caused by the error amplification effect of low G value for angle set #1. The harmonics of the three profiles are shown in Fig. 7c. It can be seen that the artefact profile for the first angle set shows obvious peaks at the 35 UPR and 62 UPR, which agrees with the low values of the weighting function.

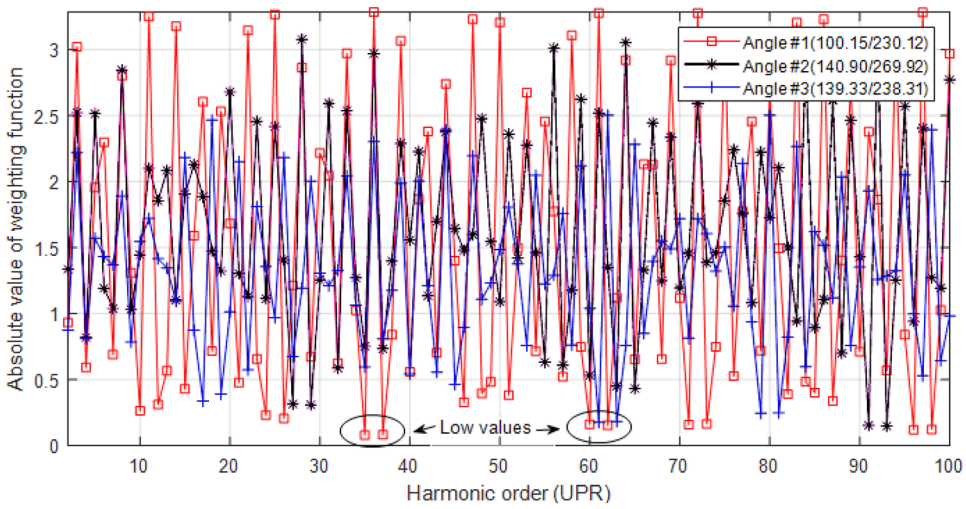

Fig. 6 Harmonic weighting functions after probe mounting

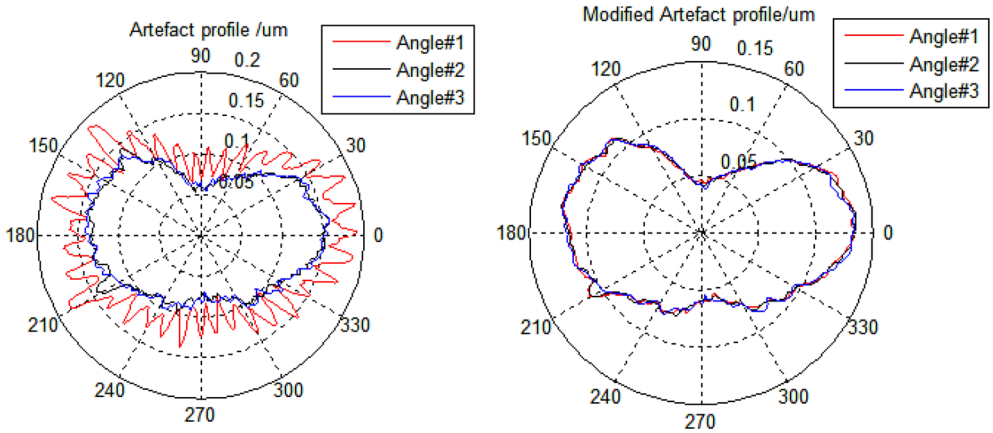

(a) Separated artefact profile without complementary method **(b)** Artefact profile with complementary method

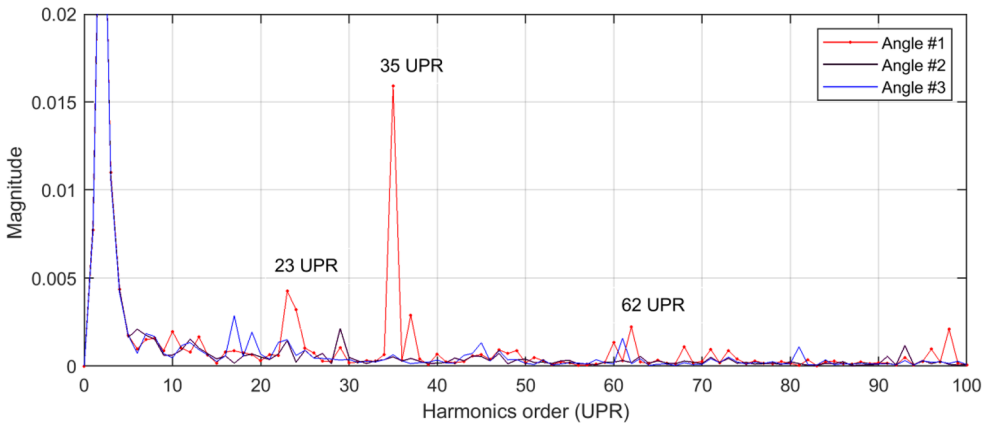

(c) Harmonics of separated artefact profile from the three angle setups without complementary method

Fig. 7 Harmonic suppression problem and the improved results with the complimentary method

Then the complementary method is applied to each curve to address this problem. The magnitude of the artefact profile spectrum is scaled to be the smallest of the three. In this case, the phase of each separated profile is kept unchanged for each angle set. Thus three results for the artefact shape are obtained only with phase differences. The modified

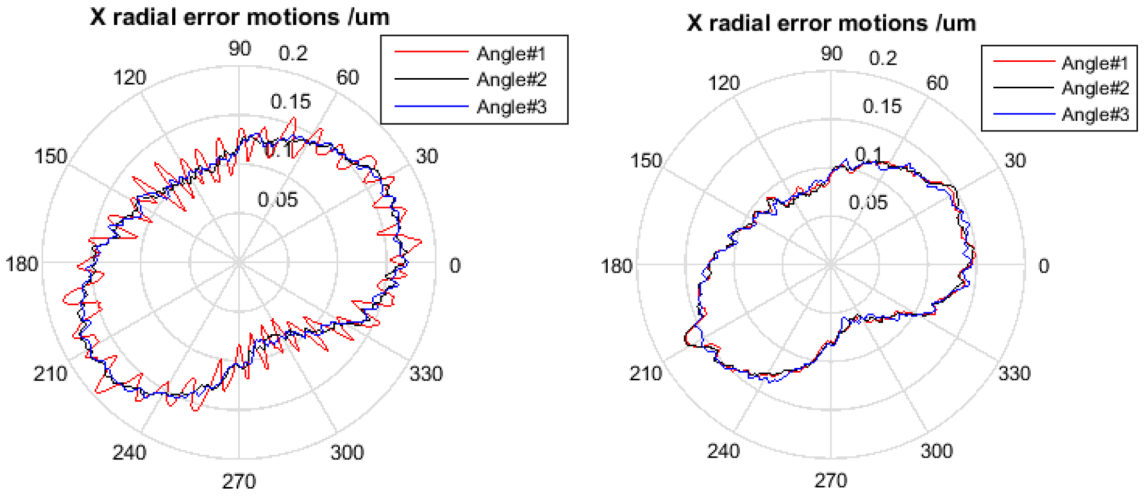

(a) Results without complementary method **(b)** Results with complementary method

Fig. 8 Comparison of *X* radial results with and without complementary method

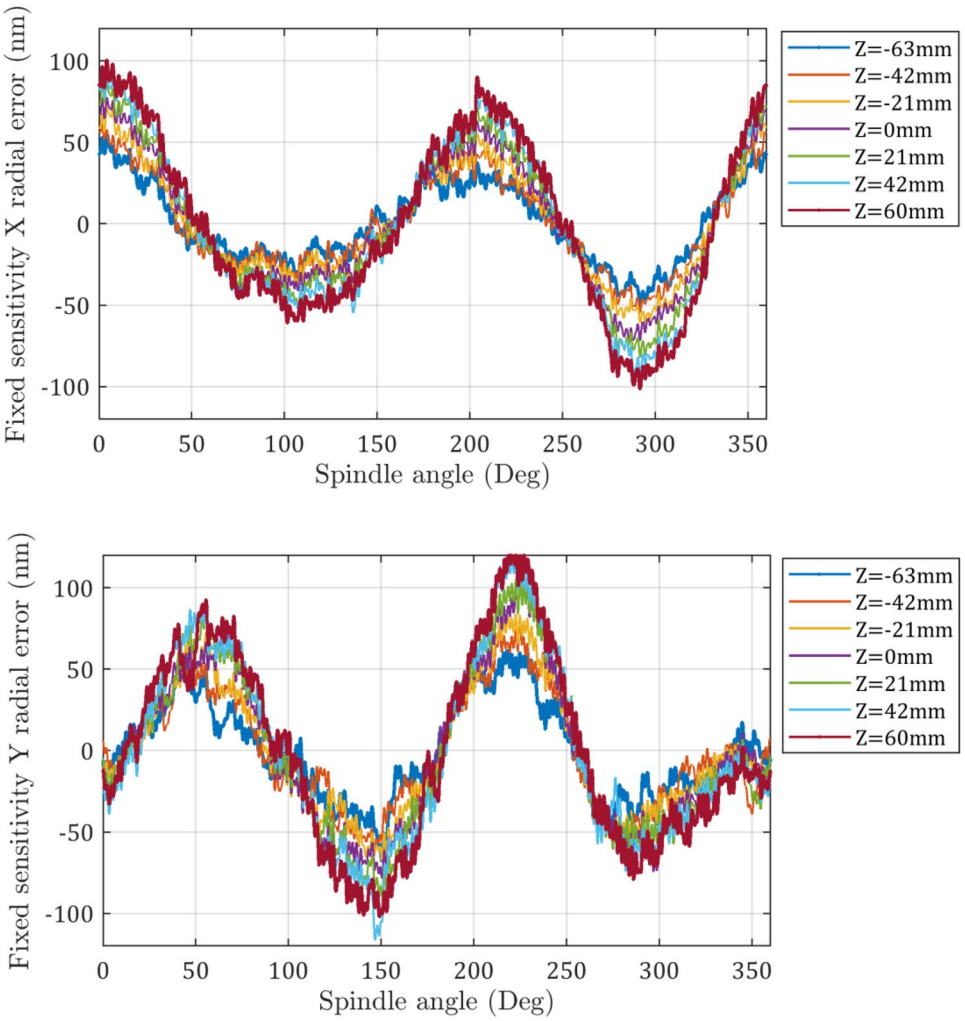

Fig. 9 Fixed-sensitivity radial error motions (*X* and *Y*) measured at different axial locations

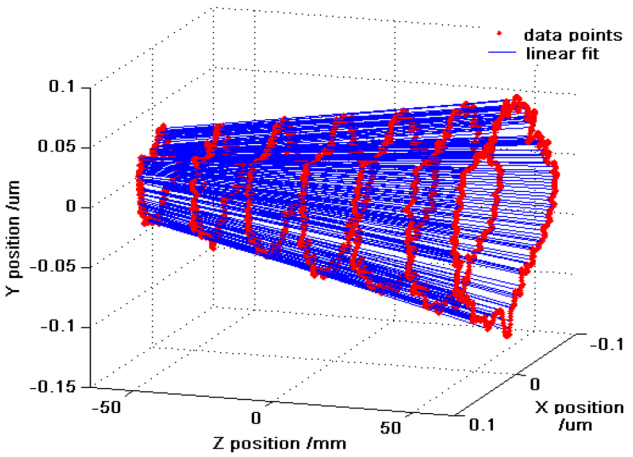

Fig. 10 Trajectories of spindle rotating center line with linear-fitted data

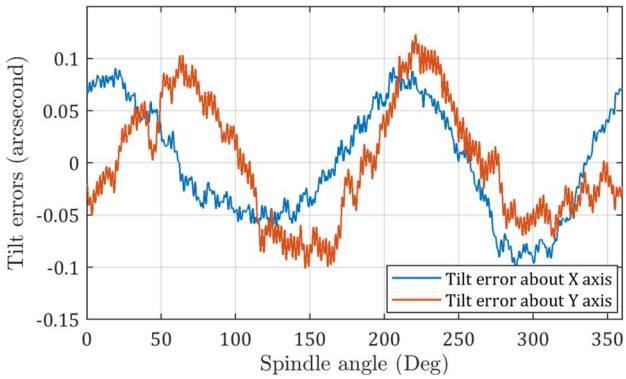

Fig. 11 Calculated tilt errors about the X and Y axis in one full spindle revolution

artefact profiles are shown in Fig. 7b and the results show that the maximum differences between the three measurements are reduced from 24.1 to 7.3 nm, thus the harmonic problem is effectively reduced by 70% in this case. The modified results possess greatly improved agreement between the three measurements. The averaged results of the three curves are deemed as the artefact profile error.

The fixed-sensitivity error motion along the X direction is calculated according to Eq. (12). Figure 8a, b shows the synchronous X radial error motions with and without the complementary method. Again, the revised results possess much improved agreement between the three measurements. The peak-to-peak synchronous X-axis radial error is measured to be 108.1, 112.1, and 101.1 nm, respectively.

4.3 Measurement of Spindle Tilt Error Motions

Radial error motions at different axial locations (from $Z=-63$ mm to $Z=60$ mm for every 21 mm) are measured using the above method. The X and Y radial error motions are shown in Fig. 9. It can be seen that the major components of the radial errors are the twofold undulations. As the measurement axial locations is further from the bearing location ($Z=-63$ mm), the peak-to-peak X radial error gets larger and larger. The same trend also applies in the Y direction.

The rotating-sensitivity spindle error is calculated by the square root of the summed X and Y radial errors. The rotating-sensitivity spindle error indicates the trajectories of the rotating center in Cartesian coordinate. Linear curve fit is applied at each rotary position and the results are plotted in Fig. 10. The measured trajectories at different axial locations show good linear relationship and this further verified that the error separation method is reliable.

The fitted lines are then used to calculate the tilt errors of the spindle. The measured tilt errors are shown in Fig. 11. The angular deviations about the X and Y axis are within ± 0.1 arc-seconds for the full spindle revolution.

5 Conclusions

In this paper, a complementary multi-probe method is proposed for in situ measurements of spindle error motions with the reduction of harmonic suppression effects. Measurements at three sets of optimized angles reveals different harmonic estimations of the artefact form profile. Both the separated artefact circularity error and the derived radial errors show good agreement for repeated measurements and the harmonic suppression effect is reduced by 70%. The influences of the erroneous harmonics at 35 and 62 UPR are successfully reduced. The tilt error motions of the spindle are obtained by measuring the radial error motions at seven axial locations. The amplitude of the radial error increases linearly with the axial location from the bearing point, which showed that the spindle errors are successfully separated from the artefact errors.

Acknowledgements The authors gratefully acknowledge the financial support from the UK Engineering and Physical Sciences Research Council (EPSRC) [EP/K018345/1]; and a joint John Anderson PhD studentship provided by DePuy (Ireland) and the University of Strathclyde [S150852] for this study. The first author also wants to thank China Scholarship Council for providing a stipend.

Data Statement All data underpinning this publication are openly available from the University of Strathclyde Knowledge Base.

References

1. Choi J-P, Lee S-J, Kwon H-D (2003) Roundness error prediction with a volumetric error model including spindle error motions of a machine tool. Int J Adv Manuf Technol 21:923–928. https://doi.org/10.1007/s00170-002-1407-y
2. Chen G, Sun Y, Zhang F, An C, Chen W, Su H (2017) Influence of ultra-precision flycutting spindle error on surface frequency domain error formation. Int J Adv Manuf Technol 88:3233–3241. https://doi.org/10.1007/s00170-016-9024-3
3. Grejda R, Marsh ER, Vallance RR (2005) Techniques for calibrating spindles with nanometer error motion. Precis Eng 29:113–123. https://doi.org/10.1016/j.precisioneng.2004.05.003
4. Whitehouse DJ (1976) Some theoretical aspects of error separation techniques in surface metrology. J Phys E 9:531–536. https://doi.org/10.1088/0022-3735/9/7/007
5. Evans CJ, Hocken RJ, Estler WT (1996) Self-calibration: reversal, redundancy, error separation, and "absolute testing". CIRP Ann Manuf Technol 45:617–634. https://doi.org/10.1016/S0007-8506(07)60515-0
6. Lee JC, Gao W, Shimizu Y, Hwang JH, Oh JS, Park CH (2012) Spindle error motion measurement of a large precision roll lathe. Int J Precis Eng Manuf 13:861–867. https://doi.org/10.1007/s12541-012-0112-5
7. Marsh ER, Arneson DA, Martin DL (2010) A comparison of reversal and multiprobe error separation. Precis Eng 34:85–91. https://doi.org/10.1016/j.precisioneng.2009.03.001
8. Moore D (1989) Design considerations in multiprobe roundness measurement. J Phys E 22:339–343. https://doi.org/10.1088/0022-3735/22/6/001
9. Zhang GX, Wang RK (1993) Four-point method of roundness and spindle error measurements. CIRP Ann 42:593–596. https://doi.org/10.1016/S0007-8506(07)62517-7
10. Zhang GX, Zhang YH, Yang SM, Li Z (1997) A multipoint method for spindle error motion measurement. CIRP Ann 46:441–445. https://doi.org/10.1016/S0007-8506(07)60861-0
11. Chen Y, Zhao X, Gao W, Hu G, Zhang S, Zhang D (2017) A novel multi-probe method for separating spindle radial error from artifact roundness error. Int J Adv Manuf Technol 93:623–634. https://doi.org/10.1007/s00170-017-0533-5
12. Linxiang C, Hong W, Xiongua L, Qinghong S (1992) Full-harmonic error separation technique. Meas Sci Technol 3:1129–1132. https://doi.org/10.1088/0957-0233/3/12/002
13. Cappa S, Reynaerts D, Al-Bender F (2014) Reducing the radial error motion of an aerostatic journal bearing to a nanometre level: theoretical modelling. Tribol Lett 53:27–41. https://doi.org/10.1007/s11249-013-0241-8
14. Cappa S, Reynaerts D, Al-Bender F (2014) A sub-nanometre spindle error motion separation technique. Precis Eng 38:458–471. https://doi.org/10.1016/j.precisioneng.2013.12.011
15. Shi S, Lin J, Wang X, Zhao M (2016) A hybrid three-probe method for measuring the roundness error and the spindle error. Precis Eng 45:403–413. https://doi.org/10.1016/J.PRECISIONENG.2016.03.020
16. Shi S, Zhang H, Qu J, Jin G, Kuschmierz R, Czarske J (2019) Measurement uncertainty propagation in spindle error separation techniques—investigation by means of stochastic spectral method. Int J Mach Tools Manuf 141:36–45. https://doi.org/10.1016/J.IJMACHTOOLS.2019.03.006
17. Zhao W, Tan J, Xue Z, Fu S (2005) SEST: a new error separation technique for ultra-high precision roundness measurement. Meas Sci Technol 16:833–841. https://doi.org/10.1088/0957-0233/16/3/027
18. Tong S (1996) Two-step method without harmonics suppression in error separation. Meas Sci Technol 7:1563–1566. https://doi.org/10.1088/0957-0233/7/11/003
19. Gao W, Kiyono S, Nomura T (1996) A new multiprobe method of roundness measurements. Precis Eng 19:37–45. https://doi.org/10.1016/0141-6359(96)00006-2
20. Gao W, Kiyono S, Sugawara T (1997) High-accuracy roundness measurement by a new error separation method. Precis Eng 21:123–133. https://doi.org/10.1016/S0141-6359(97)00081-0
21. Gao W, Kiyono S, Satoh E, Sata T (2002) Precision measurement of multi-degree-of-freedom spindle errors using two-dimensional slope sensors. CIRP Ann 51:447–450. https://doi.org/10.1016/S0007-8506(07)61557-1
22. Liu C-H, Jywe W-Y, Lee H-W (2004) Development of a simple test device for spindle error measurement using a position sensitive detector. Meas Sci Technol 15:1733–1741. https://doi.org/10.1088/0957-0233/15/9/009
23. Vissiere A, Nouira H, Damak M, Gibaru O, David JM (2012) Concept and architecture of a new apparatus for cylindrical form measurement with a nanometric level of accuracy. Meas Sci Technol 23:094014. https://doi.org/10.1088/0957-0233/23/9/094014
24. Ashok SD, Samuel GL (2012) Modeling, measurement, and evaluation of spindle radial errors in a miniaturized machine tool. Int J Adv Manuf Technol 59:445–461. https://doi.org/10.1007/s00170-011-3519-8
25. Chen D, Fan J, Zhang F (2012) An identification method for spindle rotation error of a diamond turning machine based on the wavelet transform. Int J Adv Manuf Technol 63:457–464. https://doi.org/10.1007/s00170-012-3923-8
26. Ma P, Zhao C, Lu X, Gong C, Niu X (2014) Rotation error measurement technology and experimentation research of high-precision hydrostatic spindle. Int J Adv Manuf Technol 73:1313–1320. https://doi.org/10.1007/s00170-014-5905-5
27. Shu Q, Zhu M, Liu X, Cheng H (2017) Radial error motion measurement of ultraprecision axes of rotation with nanometer level precision. J Manuf Sci Eng 139:071017. https://doi.org/10.1115/1.4036349
28. Tu JF, Bossmanns B, Hung SCC (1997) Modeling and error analysis for assessing spindle radial error motions. Precis Eng 21:90–101. https://doi.org/10.1016/S0141-6359(97)00065-2